國立臺灣大學物理學研究所

碩士論文

Department of Physics

College of Science

National Taiwan University

Master Thesis

拉曼影像系統之設計及架設

Design and Construction of a Raman Imaging System

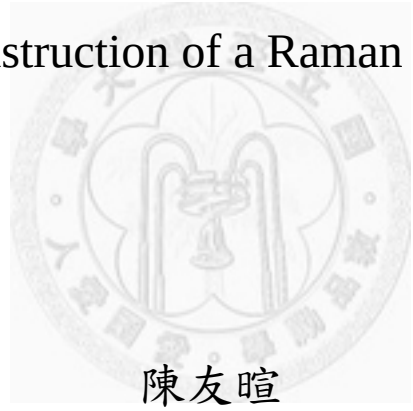

陳友暄

Yu-Hsuan Chen

指導教授：王玉麟 博士

Advisor: Yuh-Lin Wang, Ph.D.

中華民國 100 年 1 月

January, 2011

誌謝

這個部份雖然不計入口試成績，卻是不可或缺的，希望可以在我有限的字彙裡面，讓你們了解在我嘻皮笑臉的外表底下是充滿著感激。

能夠完成這篇論文，首先要感謝我的指導教授王玉麟老師。除了給予我們豐富的資源和研究上的指導，也教導我們邏輯的判斷，甚至還讓我們學會如何用比較像是科學家的口吻在說話，而不會淪為政客。謝謝王俊凱老師在光學技術上的支援，即使我經常我犯一些連初學者都不會犯的錯誤，仍然不厭其煩的跟我解釋背後的原理。謝謝也同意在審定書上面簽名的宋克嘉老師，經過你們口試的審查，讓這一份文件有機會被保留在圖書館，而不是只有存在我自己的電腦硬碟裡面。

再來要感謝勞苦功高的行政技術人員。謝謝鄒明芬小姐幫我們打點所有大小事，包括採購的部份。如果辦法取得這些完成實驗所需要的物品和器材，有再好的想法都是空談。謝謝機械工場的何光朗先生，除了讓我畫的設計稿成為儀器中的一部份，也幫我解決了無數次技術上碰到的困難。

謝謝實驗室的夥伴們，能夠完成這一項工作都是你們的功勞，這次畢業先算我的，更高的榮耀屬於你們。謝謝明佑學長研究的精神以及生活的態度，做為我們的表率。謝謝志毅哥在百忙之中抽空幫我寫推薦信，也讓我學到了很多眉眉角角。謝謝豪哥協助我處理數據，不然我可能每天都不用睡覺了。謝謝乃瑋教導我們待人處事的道理。謝謝定宇每次都很客氣的詢問我的意見，實際上卻是在傳授我研究及寫文章的方法。謝謝摳哥維持實驗室正常的運作。謝謝小黑哥啟發我對光學及攝影的興趣。謝謝 Sharma 讓我有能力可以用英文完成報告。謝謝師詠對所有人無微不至的關心與照顧。謝謝謝斌指引我好的老師可以帶我上天堂。謝謝阿棟精心幫我打造特殊規格的樣品，跟你討論科學是一件愉悅的事。謝謝阿斯卡在我迷失在研究的路途中的時候，說出了不願面對的真相。謝謝佩弟，那一段教學相長的路程，是我最珍惜的時光。謝謝好馬跟我一起念了這麼久的研究所，你優異的表現讓我看到了畢業的曙光。謝謝勵秉均讓我的情緒有一個抒發的出口。

最後要謝謝永遠支持我，也是我最深愛的爸爸、媽媽、弟弟和女友。受限於篇幅而沒有辦法列出每一個我想要感謝的人，我會用其他方式表達。

摘要

我們在光學顯微鏡上面加裝可以透過液晶調整穿透波長的濾光器和雷射光源，完成了拉曼光譜影像系統的架設。可以在 75 微米的可視範圍之內，透過一次的測量，量到特定波長的拉曼散射在空間上的強度分佈。透過矽的拉曼光譜可以測得光譜解析度為 12 公分$^{-1}$。由聚焦離子束撞擊產生的非晶矽薄膜的邊界可以測得光學解析度為 600 奈米。相信有更多關於生物及化學的研究可以透過這一套系統來完成。

ABSTRACT

We have built a Raman imaging system expanding an optical microscope with a liquid crystal tunable filter (LCTF) and a laser source. Spatial distribution of Raman scattering in a 75um field of view can be measured in one exposure. Spectral resolution has been measured to be 12cm^{-1} as full width at half maxima (FWHM) on the Raman spectrum of silicon. Spatial resolution has been determined to be 600nm on the edge of ion-beam-induced interfacial amorphization (IBIIA) treated amorphous silicon layer. We are providing an instrument with new possibilities and methods to study biology and chemistry.

CONTENTS

LIST OF FIGURES

LIST OF TABLES

Chapter 1 Introduction

Raman scattering has been developed to be a powerful tool for chemical and biological research and application. Nevertheless, most research focus on Raman scattering spectrum collected from single laser spot. Within the good quality of spectrum, information of spatial distribution was sacrificed. In order to study detailed molecular mechanism involved in microorganism by Raman scattering, we designed a Raman imaging system. Selecting a specific Raman scattering band, we can do Raman imaging of entire microorganism at the same time. The same Raman image can be taken by a computer controlled 2-dimensional mechanical motorized stage scanning spot by spot through the entire microorganism, but takes more time and yields less spatial resolution. Since chemical reactions happen in different positions of microorganism simultaneously, the time wasted moving laser beam spot might cause the loss of these information.

Moreover, since the limitation of Raman scattering cross section contributes very weak Raman scattering signal which is difficult to be detected. The development of surface enhanced Raman scattering (SERS) is such a blessing to this field of study. Conventionally, people mix gold or silver nanoparticles into the solution of their sample, the aggregation of gold or silver nanoparticles will enhance the Raman signal. But this will produce another problem if the aggregation of gold or silver nanoparticles is not uniform, then they can only enhance Raman scattering signal of a portion of whole microorganism. For a more complete and versatile study, a label-free method would be useful to monitor each and every molecular mechanism involved in microorganism. We have developed a method to fabricate SERS substrate by depositing silver nanoparticles

array on anodized aluminum oxide (AAO) template.[1] It is uniform on the aspect of morphology, and a uniform enhancement occurring to different area of the microorganism is expected. The efficiency and reproducibility of SERS by our substrate of some molecule and microorganism sample has been shown previously, more information in spatial distribution about our SERS substrate can be done in this system.

	Raman Mapping	Raman Imaging
Laser spot size (diameter)	1um	75um
Power density (a.u.)	1	1/5000
Method to take a Raman image	Move the stage to scan spot by spot in two dimensions	One exposure
Method to take a Raman spectrum	One exposure	Scan the transparent bandwidth region of the LCTF
Pros	Better resolution on spectrum	Real time monitoring
Cons	Take more time for one image	Worse resolution in spectrum

Table 1.1 Comparison of Raman mapping and Raman imaging

Chapter 2 Instrumental Setup

A Raman imaging system expanding an Olympus optical microscope (BX51), mainly with a laser source, a liquid crystal tunable filter (LCTF) and a charge coupled device (CCD)[2] was designed. The laser light source was guided into the system by a fiber and some simple optics on the left hand side of the device in order to illuminate the sample. Several filters were placed to minimize the side-mode of incident laser light as well as blocking the reflected light lead to the detection of pure Raman scattering. The crucial point to select passing Raman scattering band is the LCTF placed on the light transmission path in front of the CCD.

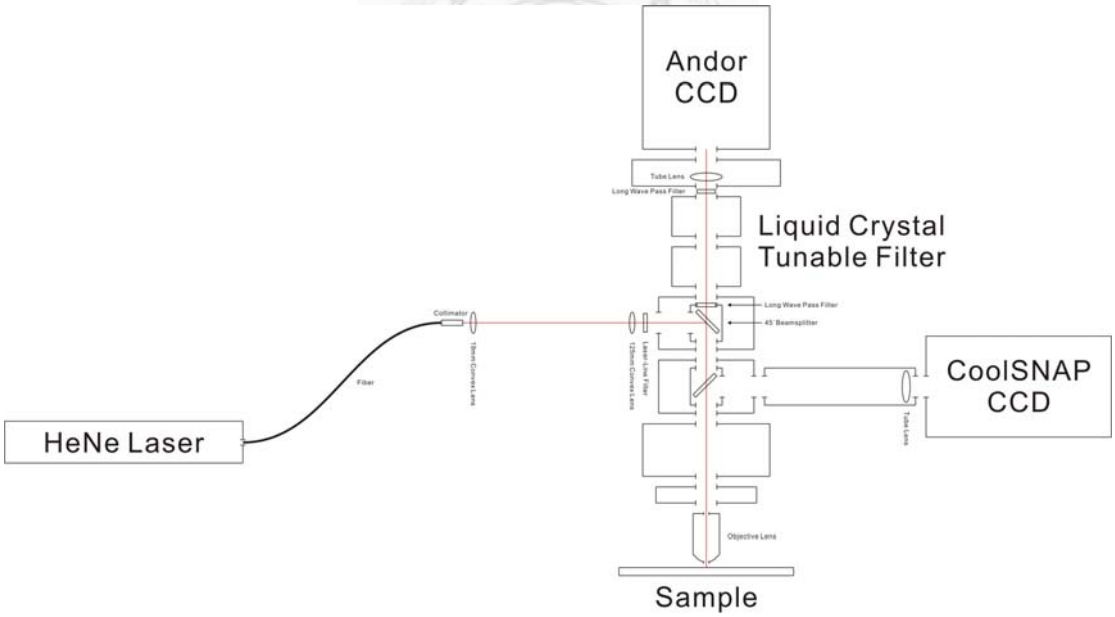

Fig. 2-1 Schematic representation of Raman imaging system

2.1 Epi-illumination

2.1.1 Laser System

For the purpose of providing photons to interact with the sample, a laser light

source is needed. In our experiment, a 632.8nm He-Ne laser from OZ Optics was selected as light source. It was coupled by a single-mode fiber and collimated with a plano-convex lens with 4.6mm focal length. The power measured after the collimator was 10mW.

2.1.2 Laser Illumination

To get a large area illuminated, the laser beam spot is expanded as large as the 75um field of view.[3] To attain this purpose, a combination of a bi-convex lens with focal length equal to 19mm and a plano-convex lens with focal length equals to 100mm are chosen. The former lens decides the angle of laser light by its position. The latter lens focuses the light on the back of the objective lens. As a result, the adjustment of laser spot size, or power density, can be made by changing the distance between the 19mm bi-convex lens and the collimator.

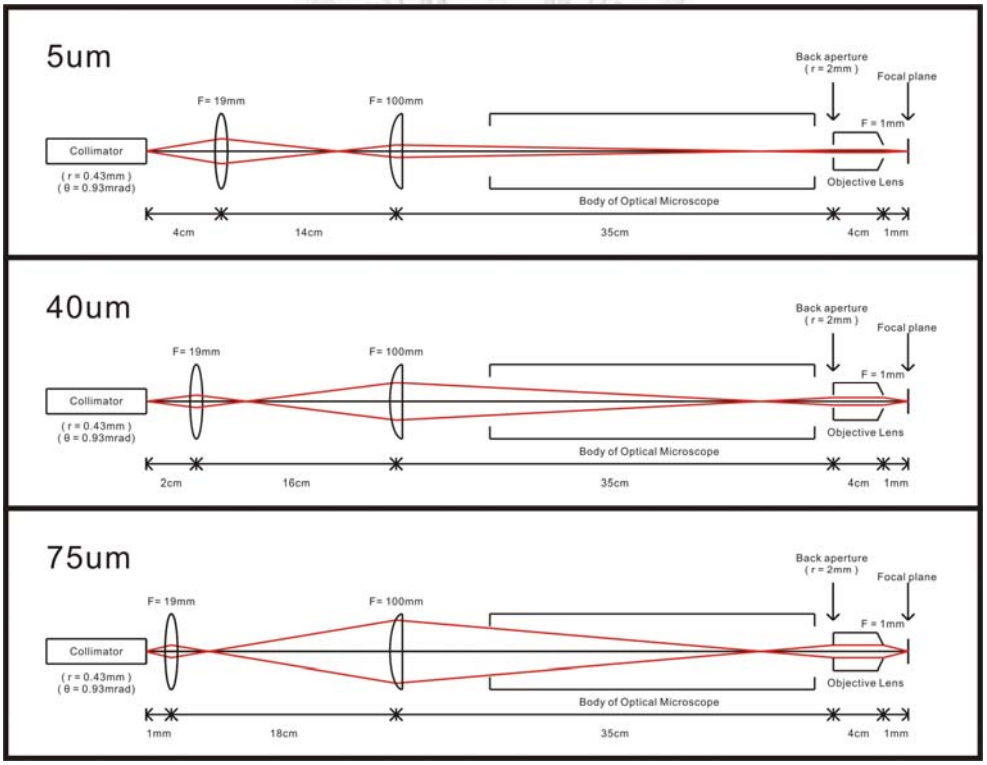

Fig. 2-2 Schematic representation of optical design for laser illumination

A 100X objective lens (MPLFLN 100X, N.A. 0.9) from Olympus was selected, and 75um beam diameter as large as the field of view was achieved. While a larger power density was required, the beam diameter could still be shrunk by decreasing the divergence angle.

2.1.3 Opto-mechanics

In order to setup the optics we need for epi-illumination, we used the design of open cage rail system. It was composed by two straight stainless rods with several open cage L-element carriers which can easily be slid or fixed on the rods.

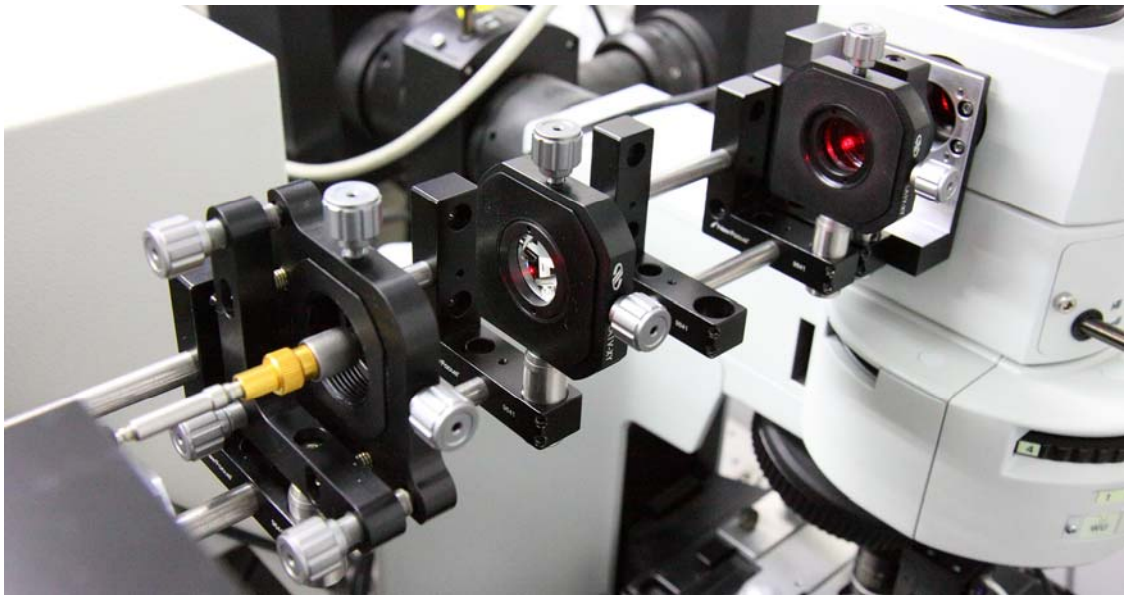

Fig. 2-3 Open cage rail system

For the connection of the open cage rail system and the optical microscope, the adapter was designed based on several purposes. There are two thread holes for the rods to lock on the left of the adapter and four counterbores for screws to lock the adapter on the body of optical microscope. The diameter of the hole in the middle is 25mm, which is enough for expanded laser light to pass. Four extra threads and set screws combination are designed for the alignment of the stainless rods or the rail.

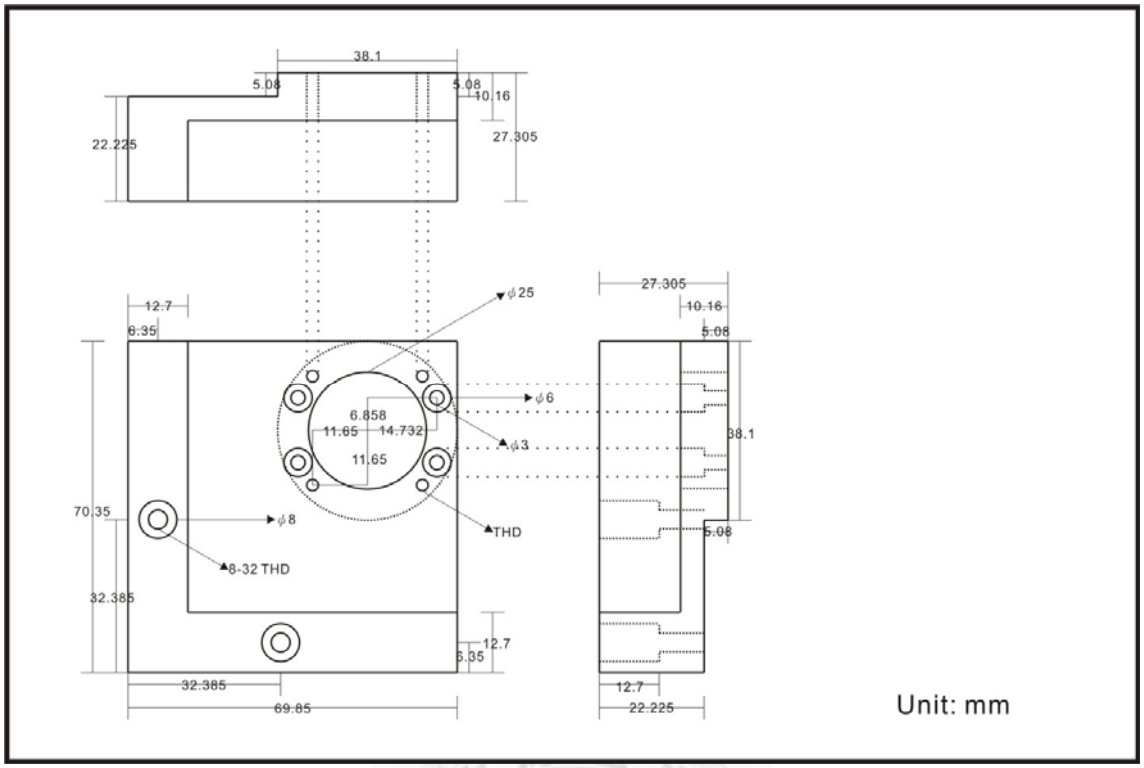

Fig. 2-4 Adapter for the open cage rail system

2.2 Clean Up the Reflected Light

Since the Raman cross section is so small and the reflected laser light may annoy the detection of Raman scattering signal, we must separate them. Taking into account that the wavelength of laser light is shorter than the wavelength of Stokes Raman scattering we are concerned, long wave pass filters are ideal to remove the reflected light. For the single wavelength light source needed in Raman scattering measurements, using laser-line filter to purify the wavelength of incident laser source was the first step. A 45° beamsplitter can reflect laser light into objective lens, and only transmit the Raman signal of sample after Stokes Raman scattering. A pair of long wave pass filters above and under the LCTF was the last protection avoiding the reflected light.

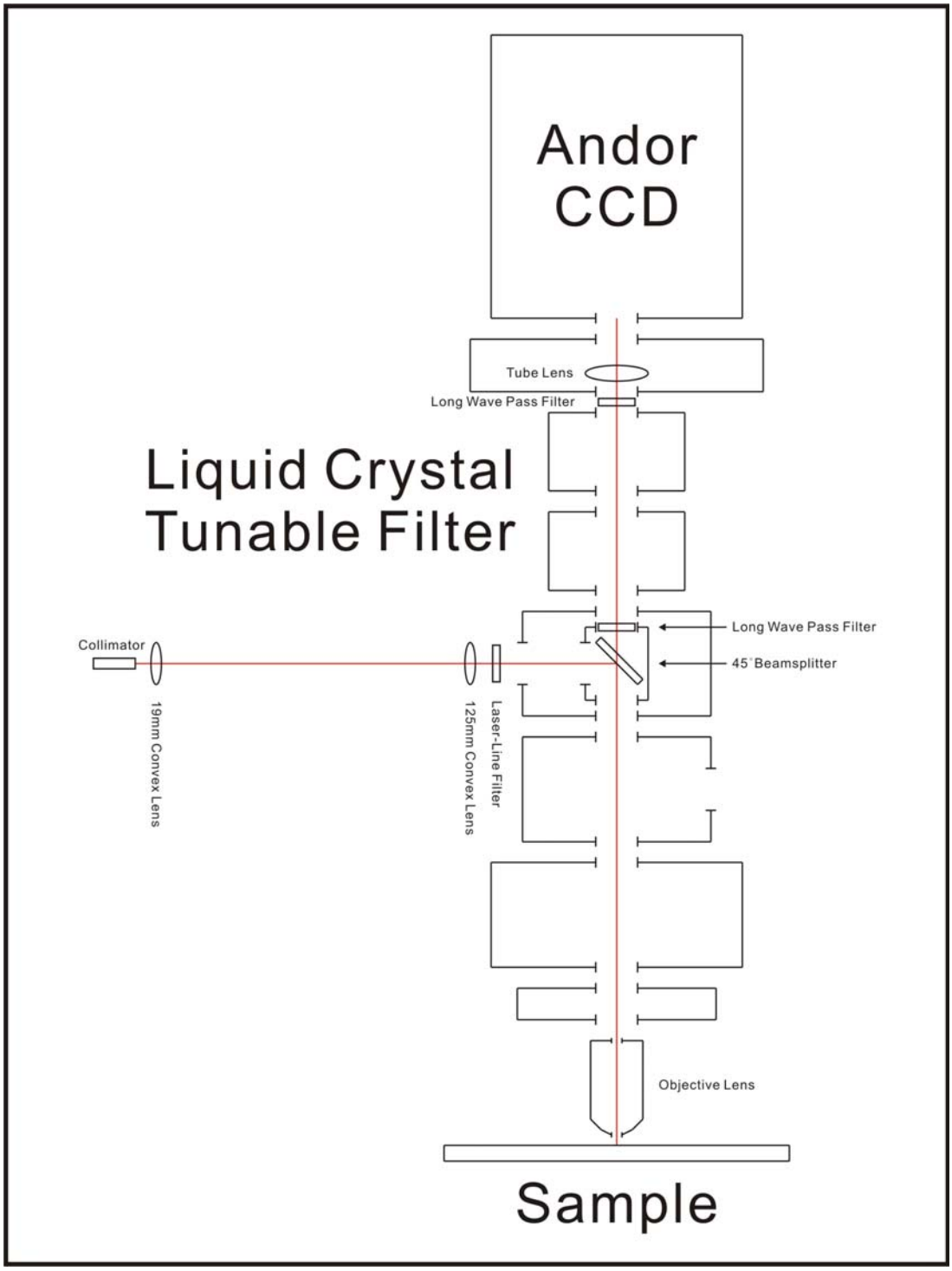

Fig. 2-5　Diagram of the filters clean up the reflected light

Long wave pass filters are powerful in filtering out the unwanted light, but only work in a limited angle of acceptance, which is around 5˚. Since the transmittance of the 45˚ beamsplitter at the wavelength of laser light (632.8nm) was 4%, there were still

a large amount of laser light that were able to transmit. After these laser light hit on the wall of the holder for the 45° beamsplitter, they will scatter in all kinds of direction and can not be totally eliminated by the long wave pass filter under the LCTF. Abnormal performances in some transparent bandwidth region of the LCTF might be caused by this kind of scattering light with large incident angle since it had already exceeded the angle of acceptance for the LCTF. In order to eliminate these random-angled scattering, an additional long wave pass filter above the LCTF was added to increased the distance between the position scattering happened and the long wave pass filter to decrease the incident angle of scattering light.

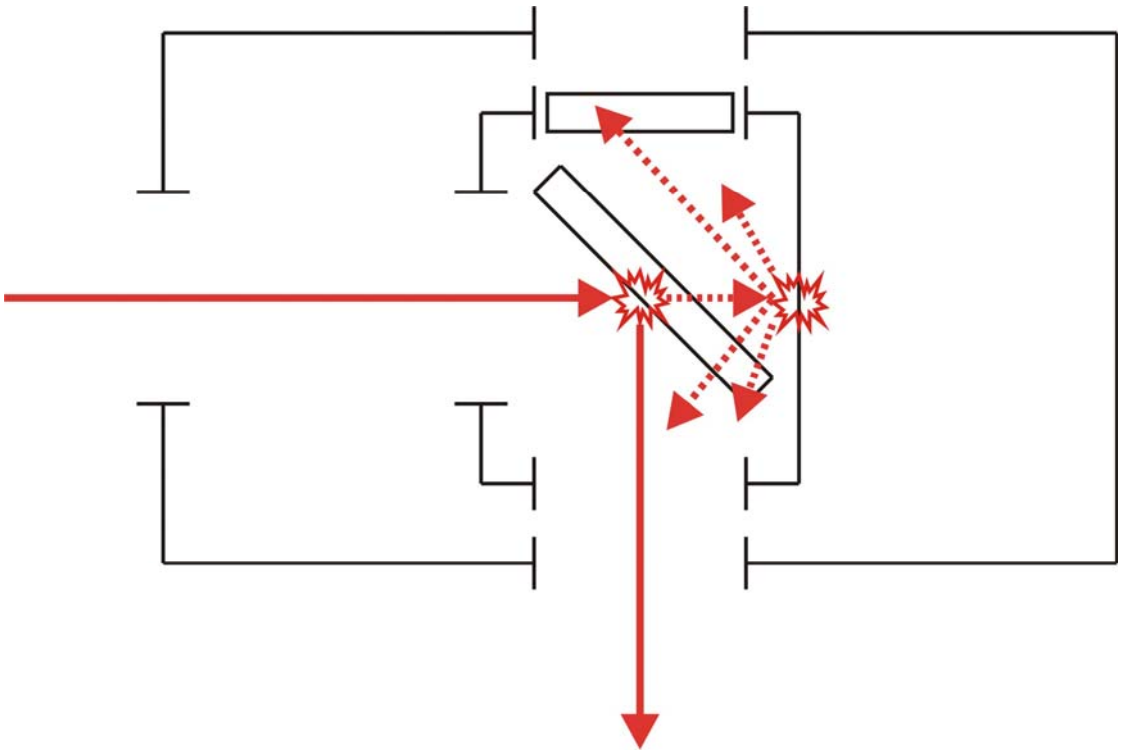

Fig. 2-6 A diagram representation of scattered laser light after it hits on the wall of the holder for the 45° beamsplitter

We selected Semrock LL01-633-25 as laser-line filter, Semrock LPD01-633RU for the 45° beamsplitter, and a pair of Semrock LP02-633RU for long wave pass filters in the optics of 633nm laser.

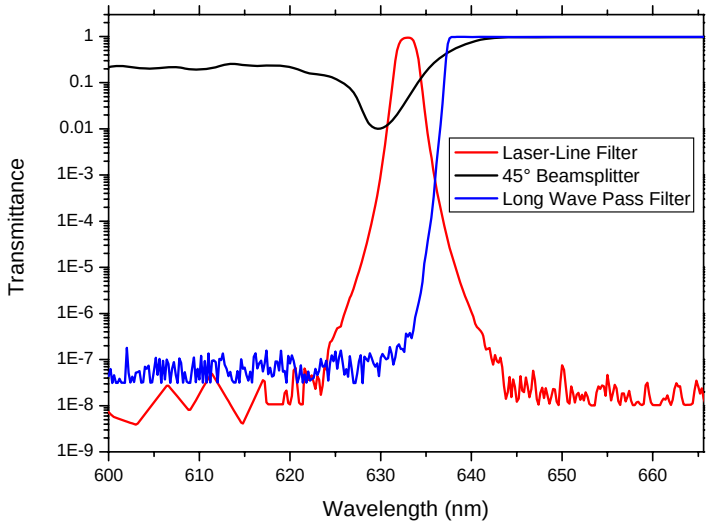

Fig. 2-7 Transmittance of filters for Raman system

2.3 Light Detection

2.3.1 Liquid Crystal Tunable Filter (LCTF)

Raman scattering happens when laser light interact with a sample, A tunable band pass filter is introduced to distinguish information from different wavelength.

VariSpec is a liquid crystal tunable filter (LCTF) manufactured by Cambridge Instrument of Research (CRi), which can tune the passing band from 550nm to 1000nm within the bandwidth of 0.75nm as full width at half maxima (FWHM). The working aperture is 22mm in diameter, and the angle of acceptance is 3.5°.

Lyot filter is a type of optical filter produces a narrow transparent bandwidth of transmitted wavelength utilizing birefringence designed by Bernard Lyot in 1933. LCTF utilizes the same concept but allows the tunability of transparent bandwidth region by adding a liquid crystal (LC) variable retarder.

A single Lyot filter stage is the combination of a retarder sandwiched by a pair of

linear polarizer, and a Lyot filter is usually built in several stages.

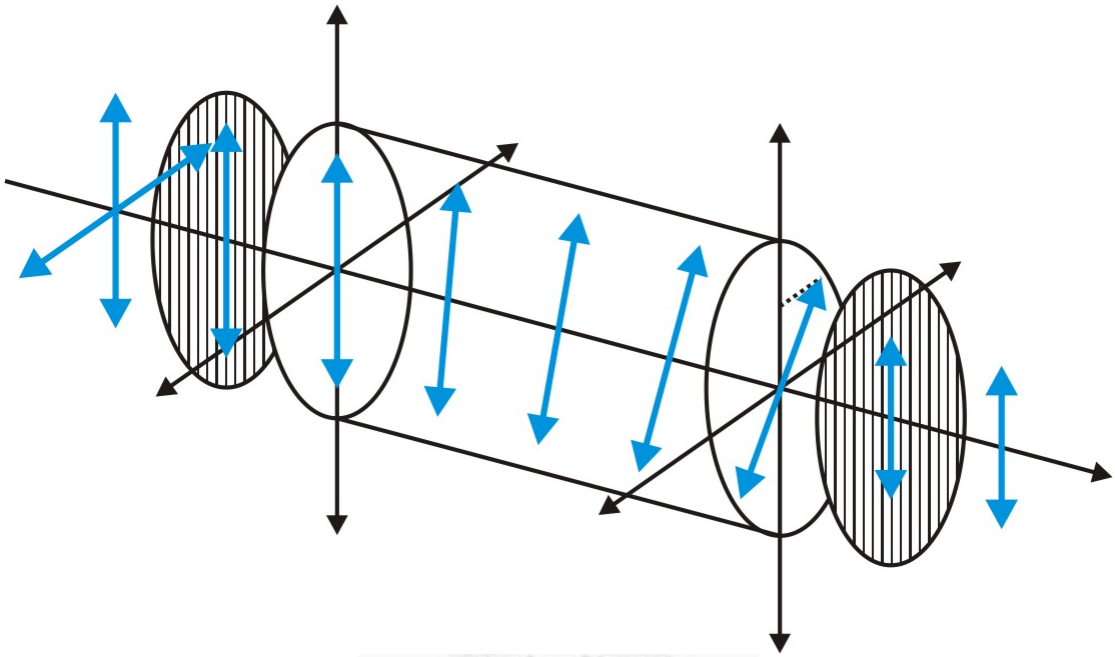

Fig. 2-8 Path of light in a single Lyot filter stage

The retarder creates a phase difference Γ between two perpendicular polarization components of the light wave by the difference in refractive index ($n(e)$-$n(o)$) following the equation:

$$\Gamma = \frac{2\pi R}{\lambda}$$

which depends on wavelength λ and retardation R:

$$R = d(n(e) - n(o))$$

d is the thickness of retarder, we can also say that the retarder shifted the direction of polarized light.

As a result, the transmittance of a single Lyot filter stage should be:

$$T = \frac{1}{2}\cos^2(\frac{\Gamma}{2})$$

obeying the Malu's Law, or:

$$T = \frac{1}{2}\cos^2(\frac{R}{\lambda}\pi)$$

which varies sinusoidally as a function of wavelength.

As a combination of single Lyot filter stages to perform a narrower transparent bandwidth, the thicknesses of retarder in different stages are often chosen in a binary sequence. There are 12 single Lyot filter stages in the VariSpec LCTF in our system, and the total transmittance is the product of every single Lyot filter stages.

Calculated result of the transmittance of LCTF combined from 1 to 6 single Lyot filter stages with retardance arranged in a binary sequence is shown in Fig. 2-9.

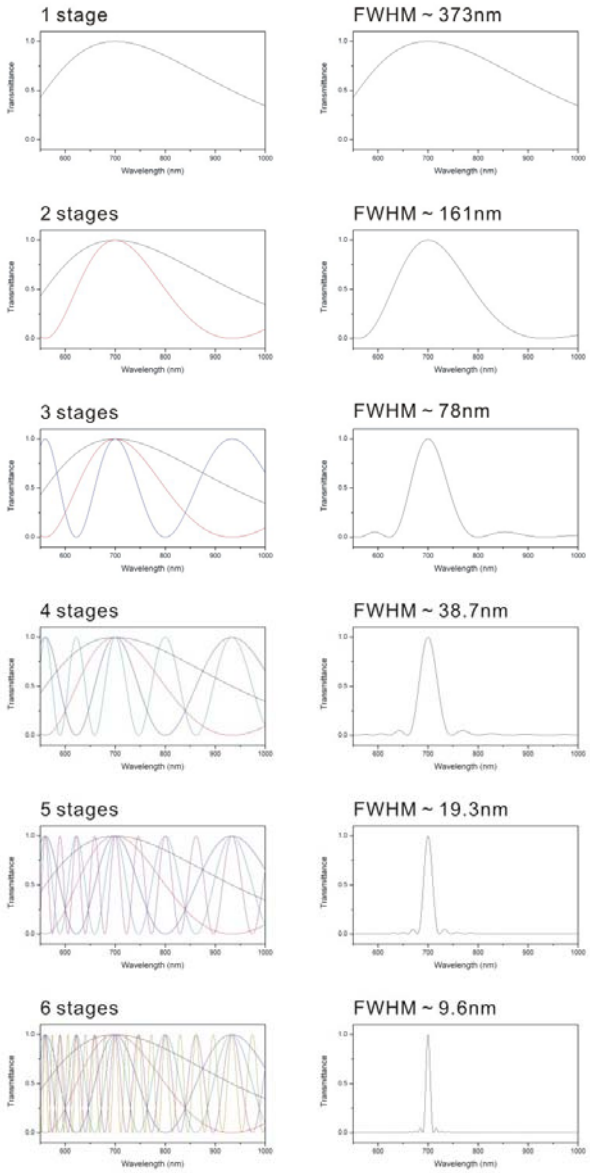

Fig. 2-9 Calculated result of the transmittance of LCTF

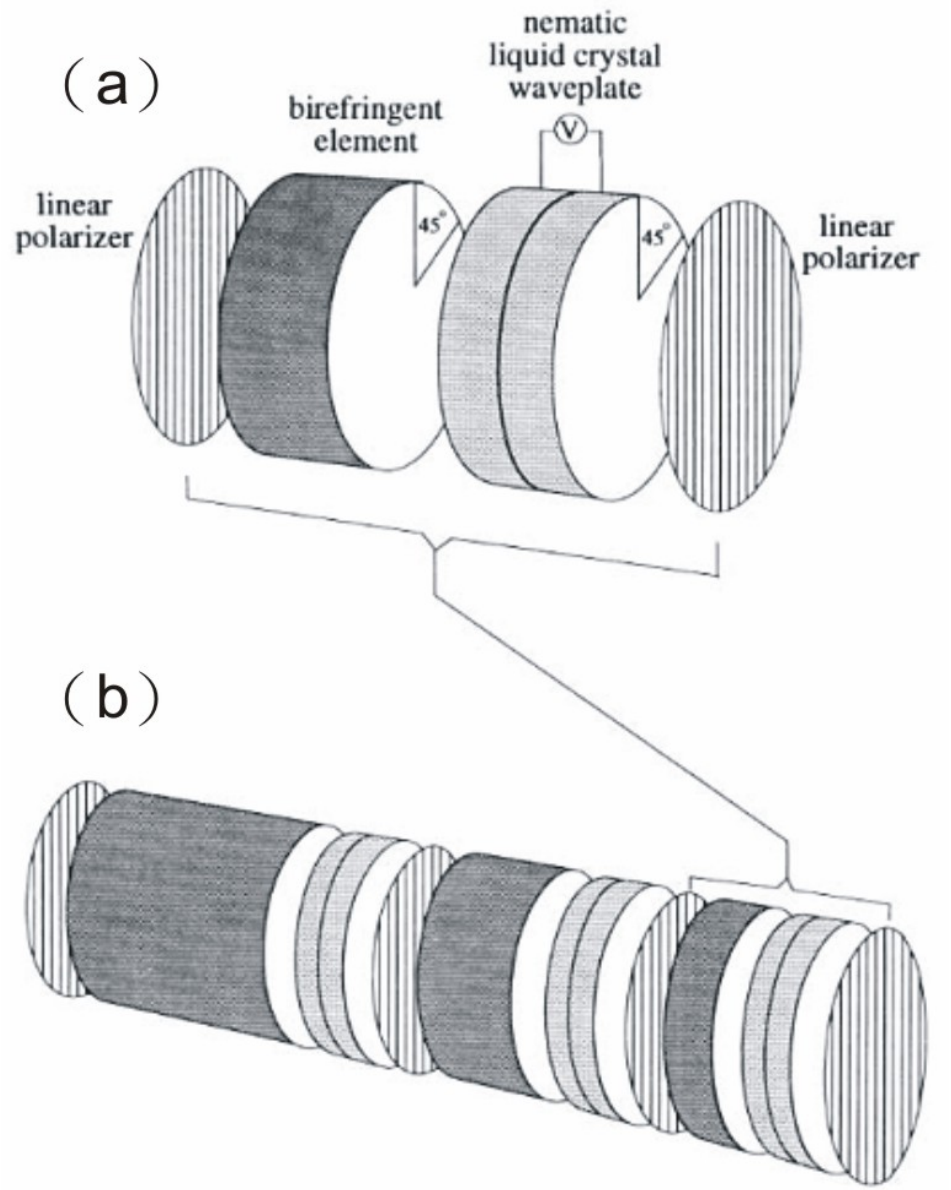

Fig. 2-10 (a) Diagram of an single stage of the LCTF (b) Diagram of a three-stage LCTF, the thicknesses of retarder in different stages are chosen in a binary sequence[3]

2.3.2 Charge Coupled Device (CCD)

For Raman imaging, we only need the CCD on the top of the LCTF, but it becomes more and more difficult to take bright field image or fluorescence image after passing the LCTF due to the narrow transparent bandwidth. So we installed another CCD for bright field imaging or fluorescence imaging.

Andor iXon DV887

The Andor iXon DV887ECS-UVB back illuminated EMCCD came from Andor Technologies and was cooled down to -50℃ in order to reduce dark current while operating. The effective size of CCD is 8.19mm x 8.19mm with 512 x 512 pixels, and the field of view is 75um x 75um under 100X objective lens. We use it as a main purpose of Raman imaging.

In order to quantify the efficiency of EM gain from the EMCCD, a calibration experiment was done with the Raman scattering signal of silicon with the transparent bandwidth region centered at 520cm^{-1}. Images are taken with 60 seconds acquisition time, and the range of EM gain was 1 ~ 255. The total counts of every pixel in the area illuminated were summed up. Fig. 2-12 and table 2.1 were drawn to compare the intensity of Raman scattering from different EM gains.

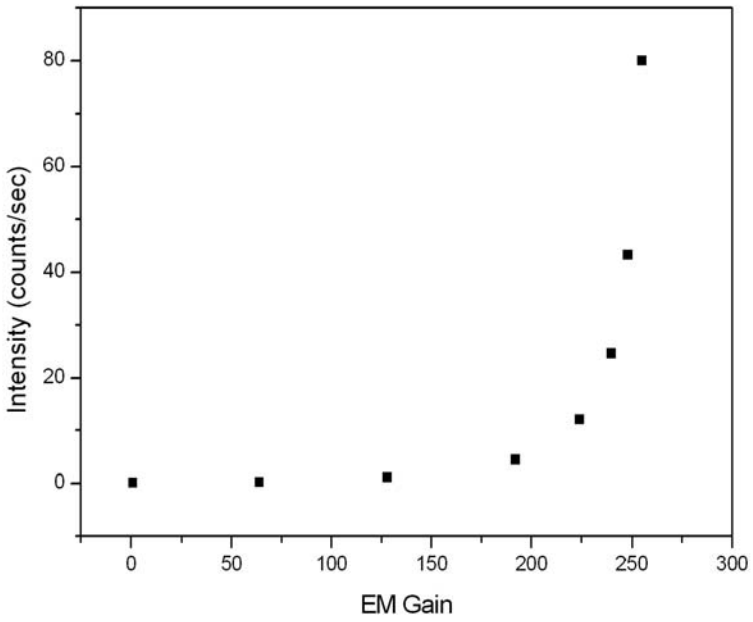

Fig. 2-11 EM Gain vs. Intensity

EM Gain	1	64	128	192	224	240	248	255
Intensity (counts)	6	16	68	270	720	1500	2600	4800
Intensity (counts/second)	0.1	0.27	1.1	4.5	12	25	43	80

Table 2.1 Intensity of Raman scattering under different EM gain

CoolSNAP HQ^2

The CoolSNAP HQ^2 Monochrome camera came from Photometrics and was cooled down to -30℃ while operating. Advanced interline-transfer CCD technology provides high quantum efficiency, most notably in the near-infrared (NIR) portion of the spectrum. The effective size of the CCD is 8.98mm x 6.45mm with 1392 x 1040 pixels, and the field of view is 86um x 64um under 100X objective lens. Bright field or fluorescence image can be taken.

2.4 Image Stabilization

2.4.1 C-Focus

This component is not in the optics of Raman imaging, but when images are taken in a long time, the phenomenon of focus drift keeps annoying us. The C-Focus system from Mad City Labs Inc. (MCL) provides an automatic means to eliminate microscope focus drift over long time periods. C-Focus corrects for microscope focus drift by using a high resolution (5nm) sensor system to measure the lens/sample spacing and make the necessary adjustments. The objective lens motions are accomplished with a lens

nanopositioner which is connected to the objective lens and microscope with standard threaded adapters. The full range of motion is 100um, 50um on both directions.

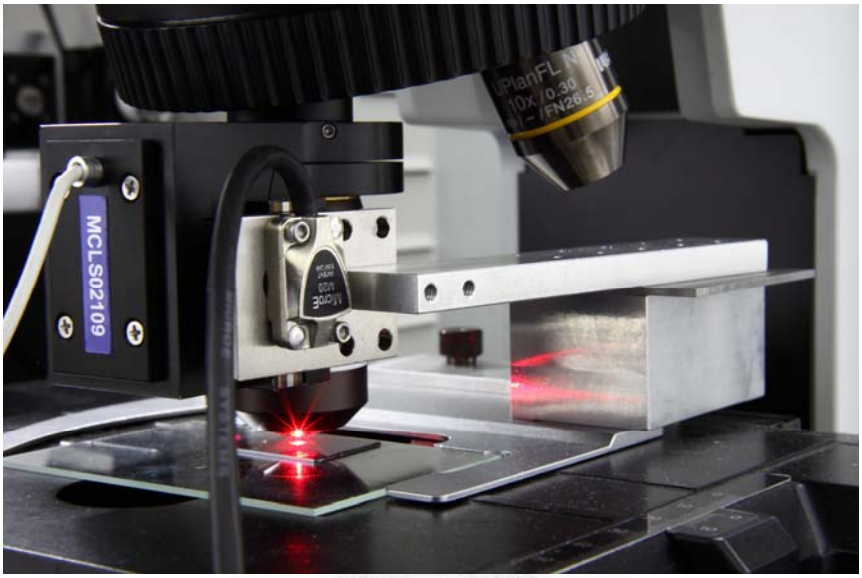

Fig. 2-12 C-Focus installed on the optical microscope

The principle of operation for C-Focus is demonstrated in Fig. 2-14. The sample on the stage should be focused manually at first like Fig. 2-14(a). After the command was delivered to the sensor locked on the stage that the stage was in focus, it starts to monitor the relative distance between the objective lens and the stage by reading the scale attached on the objective lens. Once the stage starts to drift such as Fig. 2-14(b), it was detected by the sensor reading the displacement on the scale. The piezo locked between the mount and the objective lens will compensate the displacement by its connection with the sensor through the control box, which was shown in Fig. 2-14(c). After all, although the stage may drift, the sample can still be kept in the depth of focus by the compensation from the piezo.

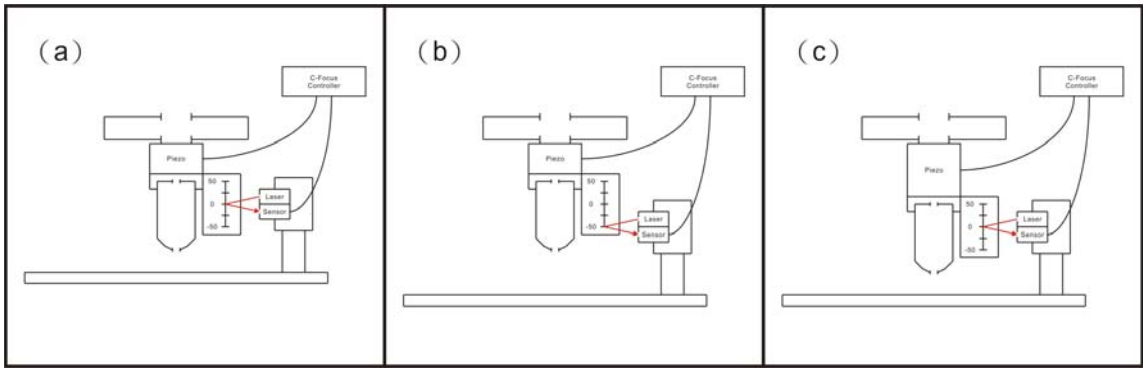

Fig. 2-13 Schematic representation of the statement of C-Focus which is (a) focus, (b) out of focus, (c) refocus

Chapter 3 Experimental Results

After the instrument was built properly, we did some demonstration about the function of this instrument and made some measurement based on the specification we designed.

3.1 Performance of the LCTF

As we mentioned above, the scattering light from the wall of the holder for the 45° beamsplitter can not be totally filtered out by the long wave pass filters under the LCTF. In order to compare the intensity of random-angled scattering light and the intensity of Raman scattering, silicon was selected to be the sample.

Three spectrums were separately drawn by scanning the center of transparent bandwidth region from 20cm^{-1} to 1900cm^{-1} with a step size of 10cm^{-1} and a summation of every pixel in each image. The acquisition time for each image was 5 seconds and the EM gain was 224. Spectrums taken with the LCTF with long wave pass filters at different positions are shown from Fig. 3-1 to Fig. 3-2.

When there is only one long wave pass filter under the LCTF as Fig. 3-4(a), an abnormal performance in some transparent bandwidth region will be caused, and the intensity is even larger than the intensity of the most prominent peak of silicon. Moving the long wave pass filter above the LCTF as Fig. 3-4(b) may improve this situation, but still not well enough. Placing long wave pass filters above and under the LCTF as Fig. 3-4(c) was the only method to operate the LCTF properly in every selected transparent bandwidth region. The image of abnormal performance when the long wave pass filter is placed under the LCTF is shown in Fig. 3-3(a). The image of abnormal performance

when the long wave pass filter is placed above the LCTF is shown in Fig. 3-3(b). The Raman image of silicon is shown in Fig. 3-3(c).

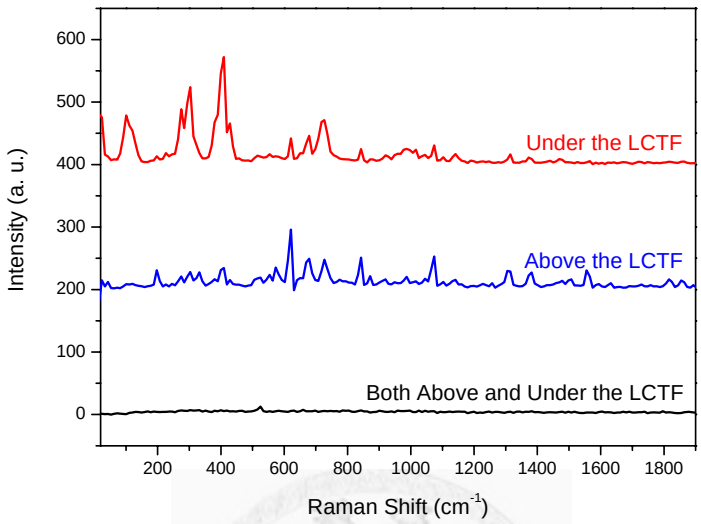

Fig. 3-1 Spectrums taken by the LCTF with long wave pass filters at different positions drawn in linear scale

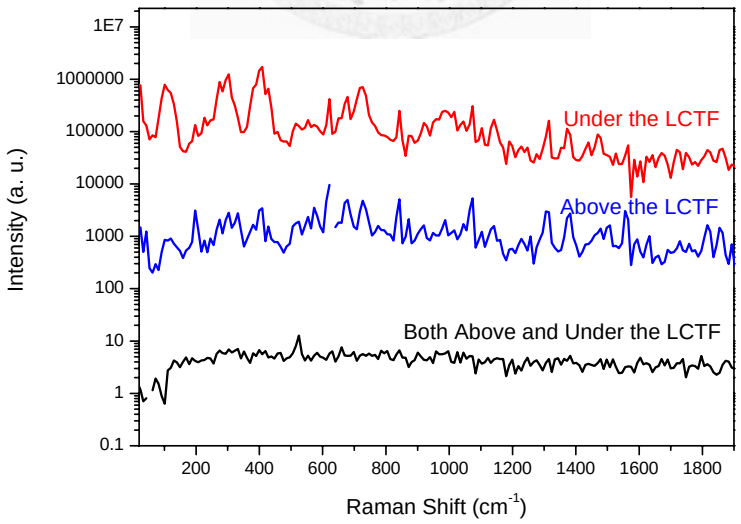

Fig. 3-2 Spectrums taken by the LCTF with long wave pass filters at different positions drawn in log scale

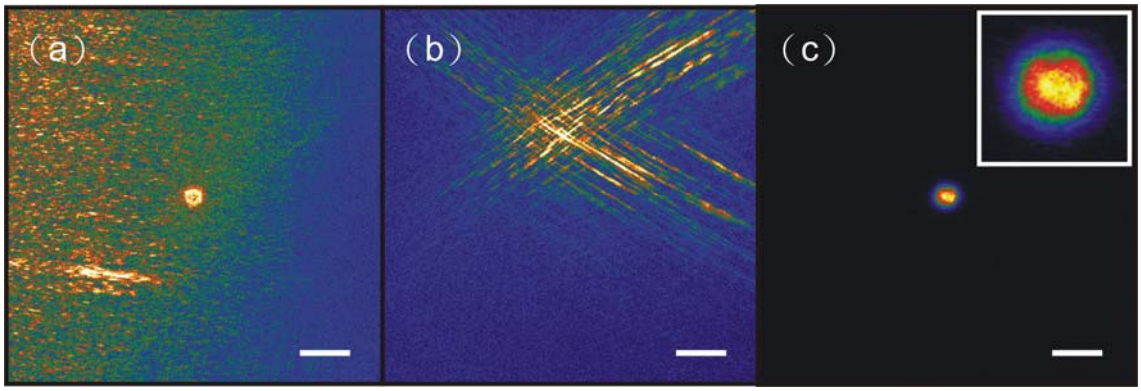

Fig. 3-3 Images taken with long pass filters (a) under the LCTF and the center of the transparent bandwidth region is selected to be 400cm-1, (b) above the LCTF and the center of transparent bandwidth region is selected to be 620cm-1, and (c) both above and under the LCTF and the center of transparent bandwidth region is selected to be 520cm-1. The scale bars are 10um long.

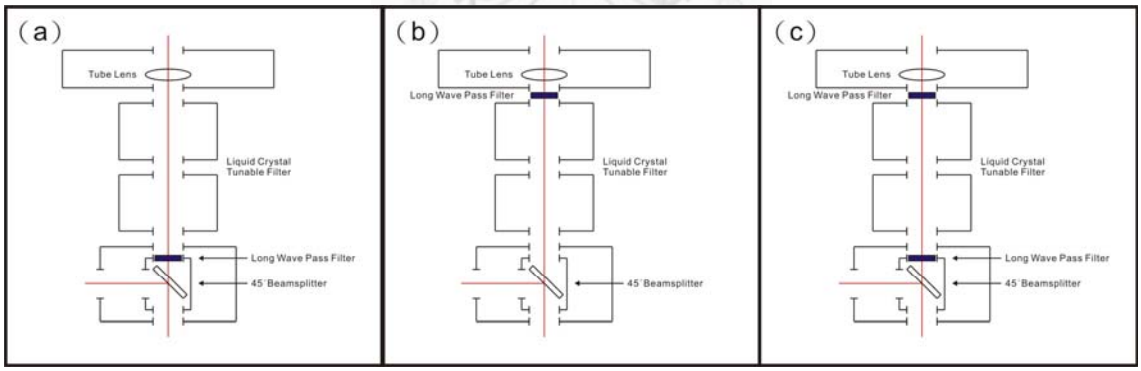

Fig. 3-4 Schematics representation of positions of long wave pass filter which are (a) under, (b) above, and (c) both above and under the LCTF

3.2 Spectrum of Silicon

Silicon has a prominent and well defined peak in Raman scattering, so it would be a good choice to use it as a calibrating sample. The Raman spectrum of silicon measured in the Raman imaging system was drawn by scanning the center of transparent bandwidth region with a step size of $10cm^{-1}$ and a summation of every pixel

on the area illuminated with laser light in each image taken with 10 seconds and 255 in EM gain. The controlled Raman spectrum of silicon for comparison was taken in a commercial Jobin Yvon Raman spectrometer with 100X objective lens and 1 second acquisition time.

Comparing Raman spectrums of silicon taken in two different instruments, not only the most prominent 520cm^{-1} peak, but also the 303cm^{-1} peak and 960cm^{-1} peak are consistent in position and relative intensity of Raman shift.

The major difference is the width of the peaks. A more precise measurement around the 520cm^{-1} peak of silicon was done by scanning the center of transparent bandwidth region with a step size of 0.5cm^{-1} in the Raman imaging system. The acquisition time was 5 seconds and the EM gain was 255. FWHM of 520cm^{-1} peak from silicon was actually 4cm^{-1}, but measured to be 12cm^{-1} in the Raman imaging system. The spectral resolution is limited by the bandwidth of the LCTF.

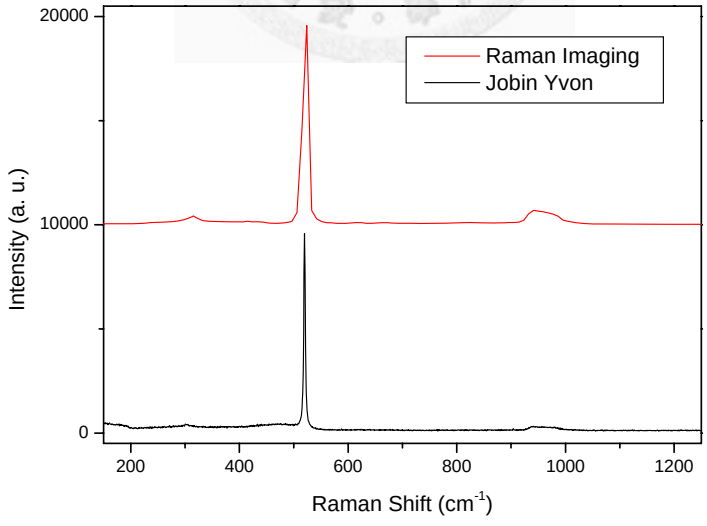

Fig. 3-5 Raman spectrum of silicon taken in Raman imaging system and Jobin Yvon Raman spectrometer

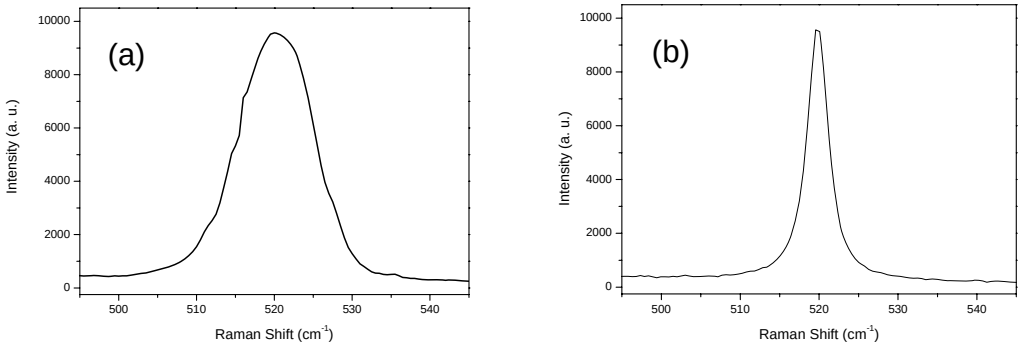

Fig. 3-6 Raman spectrum of silicon taken in (a) Raman imaging system and (b) Jobin Yvon Raman spectrometer

3.3 Amorphous Silicon

The function to measure Raman spectrum we demonstrated above is necessary but not the main purpose of building a Raman imaging system, taking Raman image is. To reduce the complexity, silicon is still chosen as sample, but a flat and uniform silicon wafer was not enough to measure the spatial resolution. Since patterns can be fabricated with high spatial resolution in focused ion beam (FIB) system, they are ideal for the measurement of spatial resolution in the Raman imaging system. Ion-beam-induced interfacial amorphization (IBIIA) treatment by gallium ion is relied to fabricate patterns of amorphous silicon layer on a silicon wafer.[5]

These patterns of amorphous silicon layer are fabricated in squares, lines, and symbols. The squares in Fig. 3-7(a) are treated by different dose from $1x10^{15}cm^{-2}$, $2x10^{15}cm^{-2}$, to $5x10^{15}cm^{-2}$ in the first row, from $1x10^{16}cm^{-2}$, $2x10^{16}cm^{-2}$, to $5x10^{16}cm^{-2}$ in the second row, and from $1x10^{17}cm^{-2}$, $2x10^{17}cm^{-2}$, to $5x10^{17}cm^{-2}$ in the last row. The length of each side is 2um. The lines in Fig. 3-7(b) are also treated by different dose, the dose of the first row is $1x10^{15}cm^{-2}$, the dose of the second row is $1x10^{16}cm^{-2}$, and the

dose of the last row $1x10^{17}cm^{-2}$. The length is 3um long with the width from 129nm, 164nm, 188nm, 350nm, to 539nm. The symbols are treated by dose of $1x10^{16}cm^{-2}$, with dimensions around 2um.

Both spectrums of crystal silicon and amorphous silicon layer are shown in Fig. 3-6. The morphology is similar, but the intensity differs. The $520cm^{-1}$ peak intensity of IBIIA treated with $1x10^{16}cm^{-2}$ dose amorphous silicon layer decreased about 40% comparing to crystal silicon.

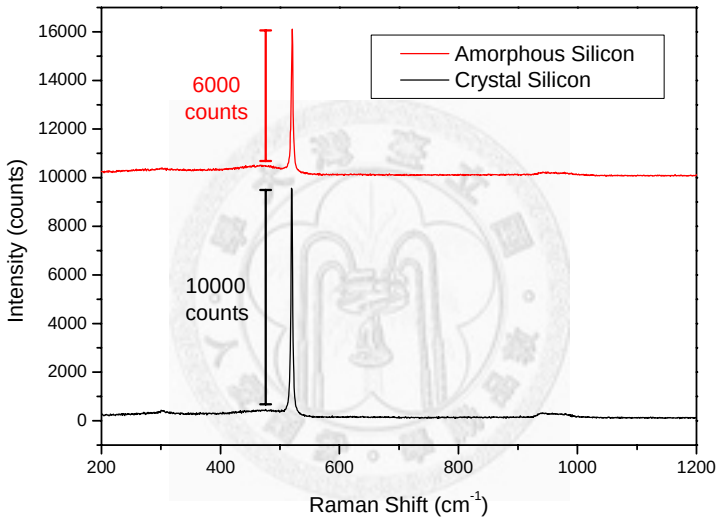

Fig. 3-7 Crystal silicon and amorphous silicon treated by FIB with $1x10^{16}cm^{-2}$ dose

The Raman images are measured in a transparent bandwidth region centered to $520cm^{-1}$, and the acquisition time is 300 seconds with 255 EM gain. From the Raman image of the Fig. 3-7(a)(iii), the intensity decayed in Raman scattering for amorphous silicon layers are proportional to the dose of gallium ion, which are consistent to their spectrum. From the Raman image of Fig. 3-7(b)(iii), the difference in width of lines are not distinguishable until the fourth line counting from the left which exceeds 350nm, and that is limited by optical resolution.

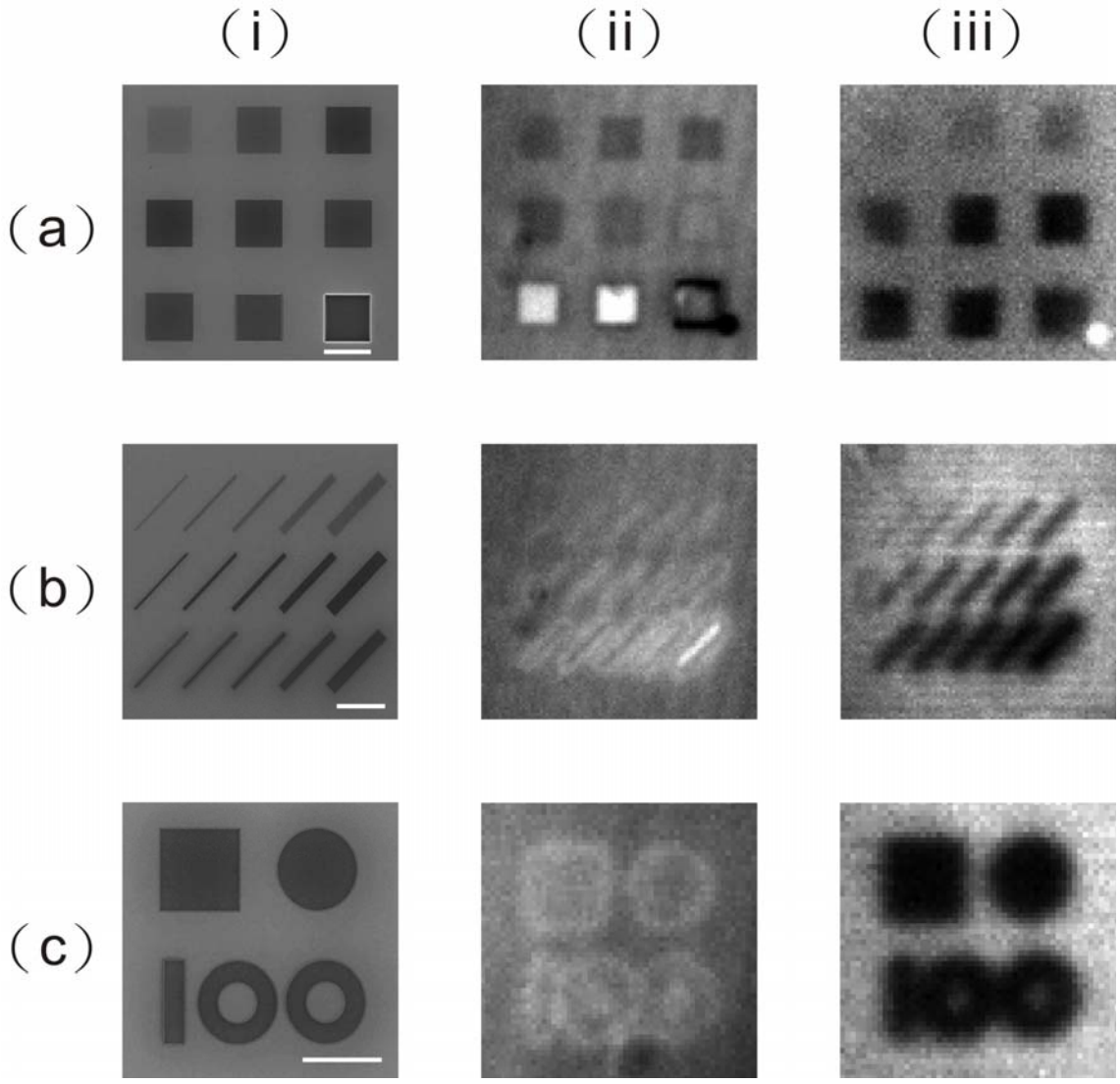

Fig. 3-8 Patterns of IBIIA treated amorphous silicon layer taken in (i) scanning electron microscopy (SEM), (ii) bright field optical microscope, and (iii) Raman imaging. The length of scale bars are 2um.

In order to measure the spatial resolution, Fig. 3-8 was cropped and magnified from Fig. 3-7(a)(iii). In the cross section of intensity from amorphous silicon layer to crystal silicon, the distance between 10% and 90% of the difference in intensity is 4±1 pixels, which represents 600±150nm.

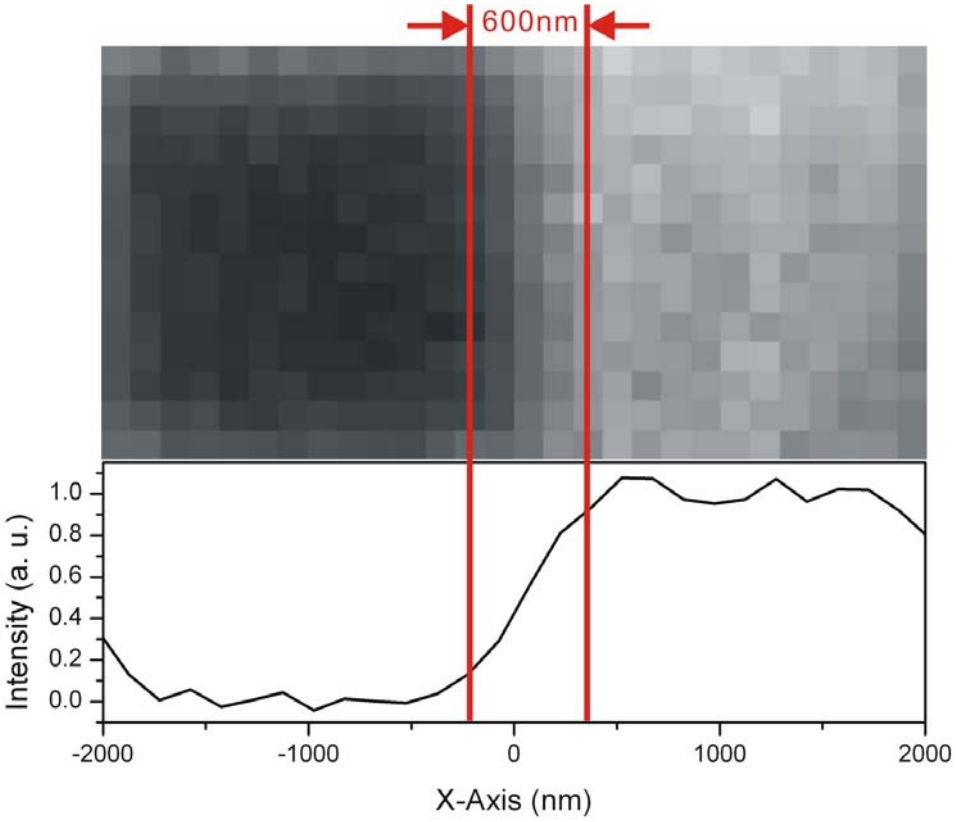

Fig. 3-9 The edge between amorphous silicon layer and crystal silicon

Chapter 4 Conclusion

A Raman imaging system with a laser, a LCTF, and a CCD have been constructed as we designed. During this process, the optics of laser has been designed to modify in an easy way. The reason the LCTF can not perform well was found and solved by realizing the principle of operation for the LCTF and adding a long wave pass filter at a different position. There is still room for improvement and research to accomplish.

4.1 Improving the Raman Imaging System

Annoying by the dark current of the CCD or the influence of the environment, it takes a long acquisition time to detect weak Raman scattering signal. A laser source with larger power will have a large benefit. For a more uniform laser illumination, well operation of a beam shaper, which can turn the distribution of laser light from a Gaussian to flat top[6] is in the technology road map. Fine tuning the calibration is going to be the last part. Since both the transmittance of LCTF and the quantum efficiency of CCD depend on wavelength, the intensity measured from the CCD need to be calibrated.

4.2 Chemical and Biological Studies

Due to its characteristic of taking Raman image in one exposure, a Raman imaging system is ideal for in situ chemical and biological studies. According to the theoretical prediction[7] and experimental calculation,[8] the enhancement factor in SERS can be less than 2.8×10^4 or more than 1×10^{10}. It will be efficient to study the distribution of SERS enhancement factor by a Raman imaging system since the intensity of SERS in

different region can be measured in one exposure. Further more, since hot junctions might blink or migrate on a SERS substrate, the motion of hot junctions can be monitored by a series of Raman images. Understanding the mechanism and behavior of SERS may help us to improve the uniformity of SERS substrate.

SERS has become a popular technique in the application of biology, gold or silver nanoparticles are also injected into microorganism samples very often. While analyzing the SERS spectrum, since the signal measured is the summation of a full microorganism, the exact position with more contribution can not be distinguished. This kind of information with spatial distribution can be measured by Raman imaging. It will be especially useful in the study about the mechanism of growing cells or the drug resistance test.

REFERENCE

[1] H. H. Wang, C. Y. Liu, S. B. Wu, N. W. Liu, C. Y. Peng, T. H. Chan, C. F. Hsu, J. K. Wang, and Y. L. Wang, Highly Raman-Enhancing Substrates Based on Silver Nanoparticle Arrays with Tunable Sub-10 nm Gaps, Adv. Mater., 18, 491-495, 2006

[2] Hannah R. Morris, Clifford C. Hoyt, Peter Miller, and Patrick J. Treado, Liquid Crystal Tunable Raman Chemical Imaging, 50, 805-811, 1996

[3] David M. Pallister and Michael D. Morris, Laser Koehler Epi-lllumination for Raman and Fluorescence Microscopic Imaging, Appl. Spectrosc, 48, 1277-1281, 1994

[4] H. Morris, C. Hoyt, and P. Treado, Imaging Spectrometers for Fluorescence and Raman Microscopy: Acousto-Optic and Liquid Crystal Tunable Filters, Appl. Spectrosc. 48, 857–866, 1994

[5] V. Heera, T. Henkel, R. Kogler, and W. Skorupa, Evidence for diffusion limited kinetics of ion-beam-induced epitaxial crystallization in silicon, Phys. Rev. B, 52, 15776-15784, 1995

[6] John A. Hoffnagle and C. Michael Jefferson, Design and performance of a refractive optical system that converts a Gaussian to a flattop beam, Appl. Opt., 39, 5488-5499, 2000

[7] E. C. Le Ru, P. G. Etchegoin, and M. Meyer, Enhancement factor distribution around a single surface-enhanced Raman scattering hot spot and its relation to single molecule detection, J. Chem. Phys., 125, 204701, 2006

[8] Ying Fang, Nak-Hyun Seong, Dana D. Dlott, Measurement of the Distribution of

Site Enhancements in Surface-Enhanced Raman Scattering, Science, 321, 388-392, 2008

SUPPORTING INFORMATION

Transmittance of the LCTF

The test data of transmittance in transparent bandwidth region was scanned by the Thermo-Nicolet spectrometer provided by CRi. Wavelength accuracy was not perfect, but within an acceptable range. Since the transmittance is not a fixed number, this is a reference for the calibration of intensity when we transform Raman image with different transparent bandwidth region to Raman spectrum.

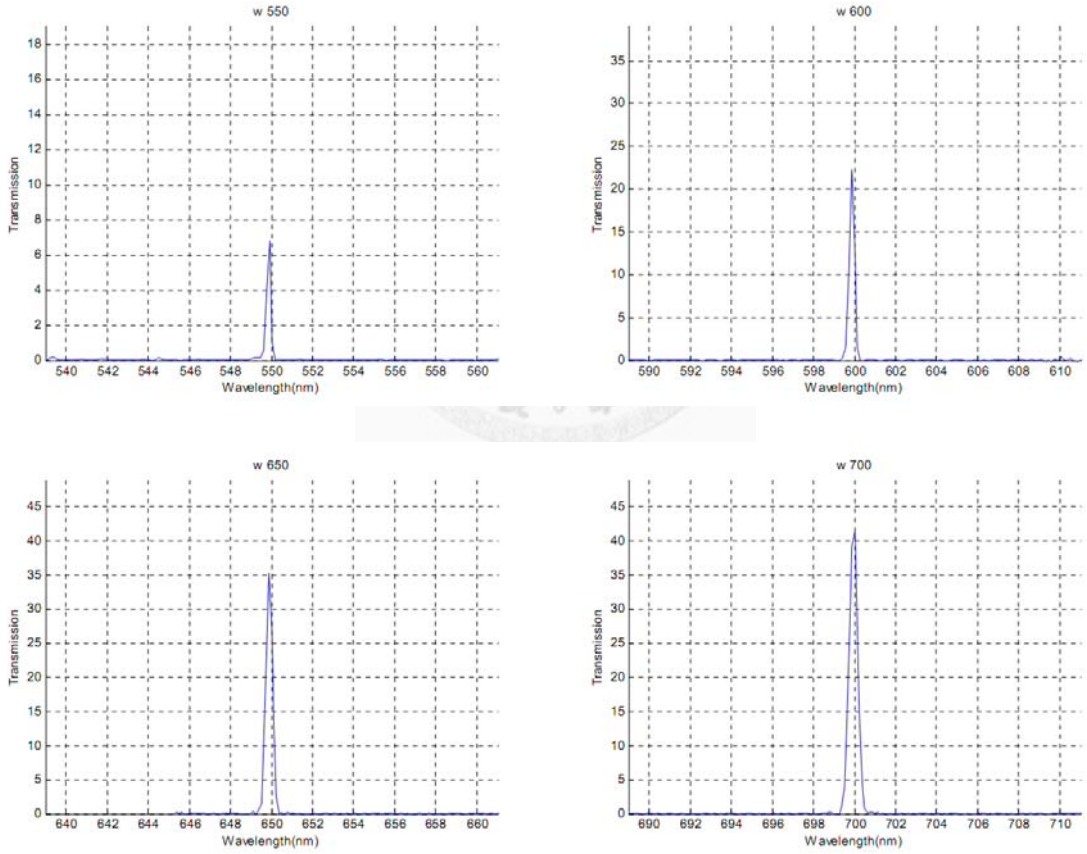

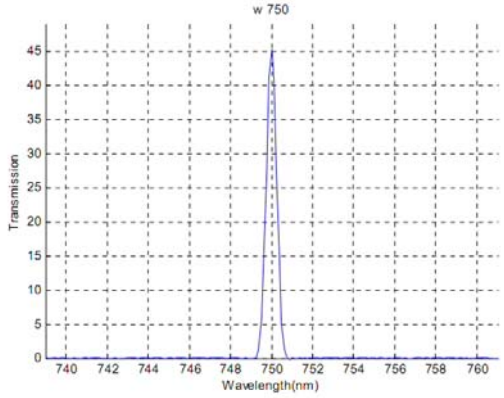
w 750
Transmission
Wavelength(nm)

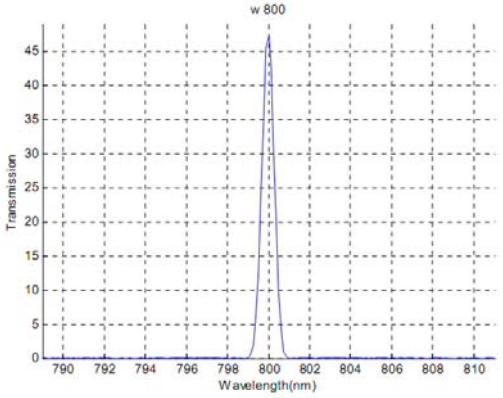
w 800
Transmission
Wavelength(nm)

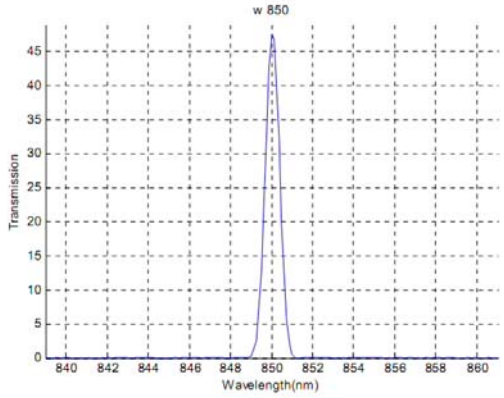
w 850
Transmission
Wavelength(nm)

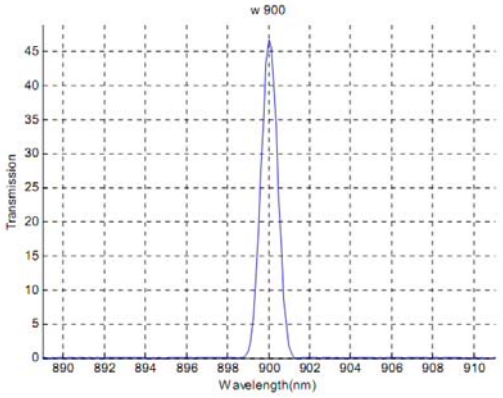
w 900
Transmission
Wavelength(nm)

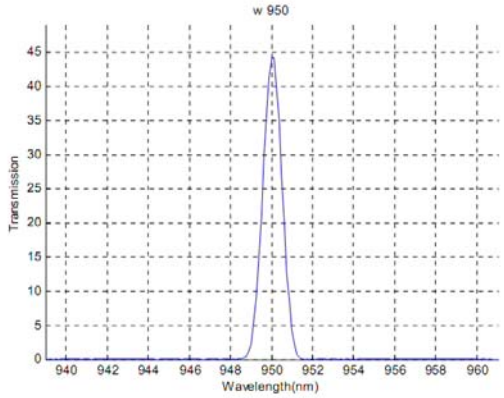
w 950
Transmission
Wavelength(nm)

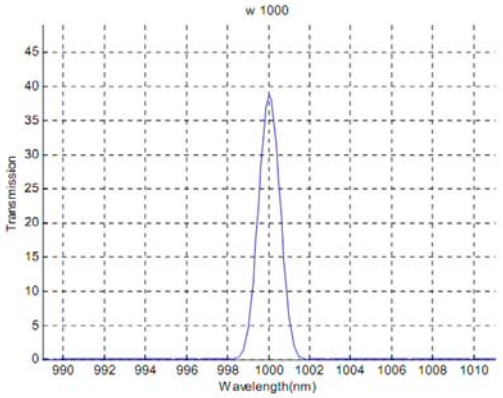
w 1000
Transmission
Wavelength(nm)